Tungsten Fluorides: Syntheses and Electrochemical Characterization in the FLINAK Molten Salt Eutectic

Sven E. Eklund, James Q. Chambers,* Gleb Mamantov,‡ Jon Diminnie, and Craig E. Barnes

Department of Chemistry, University of Tennessee, Knoxville, Tennessee 37996

Received May 8, 2000

The following tungsten fluorides have been synthesized by simple addition reactions or by reduction with tungsten metal at elevated temperature: KWF_7, K_2WF_8, MWF_6 (M = K, Na, Rb, Cs), K_2WF_7, M_3WF_8 (M = K, Na, Rb), and K_3WF_6. The compounds were characterized by their Raman spectra and by cyclic voltammetry in the molten FLINAK eutectic melt (46.5, 11.5, and 42.0 mol % of LiF, NaF, and KF, respectively) at 475−800 °C. X-ray crystal structures are reported for two new compounds K_2WF_7 and K_3WF_6. The crystals of K_2WF_7 were orthorhombic, space group *Pnma* (No. 62) with $a = 9.800(2)$ Å, $b = 5.7360(11)$ Å, $c = 11.723(2)$ Å, and $Z = 4$. Crystals of K_3WF_6 were cubic, space group $Fm\bar{3}$ (No. 225) with $a = b = c = 8.9160(10)$ Å, $Z = 4$. Electrodeposition of tungsten metal on Pt from FLINAK, prepared by the addition of WF_6 gas and metallic tungsten to the melt, is suggested to result from reduction of an equilibrium mixture of WF_8^{3-} and WF_6^{3-}.

High-temperature molten salt media are well suited to the electrolytic production of the refractory metals in groups IVA−VIA. In particular, the eutectic alkali fluoride salt mixture of LiF, NaF, and KF (46.5, 11.5, and 42.0 mol %, respectively; mp, 454 °C), also known as FLINAK, has been employed to electrodeposit all of the metals in these groups except for titanium.[1,2] Possible reasons for this behavior are the lability of the fluoride ligands and that the fluoride salt environment minimizes the formation of cluster species, as is observed when chloride is present. Molten fluoride salts have played important roles in other applications as well, including the electrowinning of aluminum from cryolite melts[3] and as homogeneous fluid fuels in molten salt nuclear reactors.[4]

Previously tungsten has been electrodeposited from FLINAK solutions containing about 1−10 wt % W that were prepared by the addition of WF_6 gas to the molten salt medium under reducing conditions.[5−7] The mean oxidation state of the electroactive species, which was reported to be +4.51 by Senderoff and Mellors[6] and +4 to +4.5 by Broc,[5] suggests the formation of either mixed-valent polynuclear species or multiple species with different oxidation states at equilibrium. A simple WF_4 species is unlikely to exist in these melts because this species is known to disproportionate to W metal and WF_6 gas at temperatures above 200−300 °C.[8]

In the course of the investigation of the tungsten electrodeposition process in FLINAK, the syntheses of several alkali salts of six-, seven- and eight-coordinate tungsten(VI) and tungsten(V) fluorides were achieved in excellent yields by simple high-temperature addition and reduction reactions using tungsten metal as the reductant. Previous synthetic methods reported for these compounds have employed iodide salts as reductants and reagents such as IF_5,[9−12] or metallocene reductants,[13] or NOF in CH_3CN.[14,15] The high-temperature routes reported here, which employ neat molten salt reactants, avoid complications due to impurities introduced by side reactions and the formation of oxyfluoride products. Raman spectra for the tungsten fluorides and a preliminary report of their electrochemical behavior in the FLINAK eutectic are presented below.

Experimental Section

General Information. All manipulations of purified chemicals and reaction products were performed in an inert atmosphere glovebox (VAC, model HE 43-2) filled with purified nitrogen and operated at <2 ppm of H_2O. KF and NaF (Fluka, >99%) were first dried at 300 °C overnight under vacuum and then recrystallized from the molten state in a glassy carbon crucible. Infrared spectra of the purified salts did not contain bands in the 3550−3700 cm^{-1} region that could be assigned to hydroxide ion. RbF(Alfa/Aesar, 99.98%), CsF(Alfa/Aesar, 99.9%), and Na_2O (Ventron, Alfa division, 98%) were used without further purification except that the former materials were dried in situ under vacuum at 600 °C for 5 h before addition of the WF_6 in the synthesis procedures. WF_6 gas (Cerac, 99.9%) and tungsten metal powder (Aesar, 99.0%, 100 and 300 mesh) were used without further purification. Elemental analysis for K was performed by E&R Microanalytical Laboratory, Inc. W was analyzed by inductively coupled plasma atomic absorption spectroscopy (ICP AAS) using $Na_2WO_4 \cdot 2H_2O$ in a NaOH solution as a standard.

The FLINAK eutectic mixture, which was supplied by L. M. Toth (ORNL), was purified by bubbling HF through the molten material at 550 °C for 3−4 days, followed by an H_2/He sparge to remove excess

‡ Deceased, March 11, 1995.

(1) Mellors, G. W.; Senderoff, S.; Canadian Patent No. 688546, 1964.
(2) Robin, A.; Ribeiro, R. B. *J. Appl. Electrochem.* **2000**, *30*, 239−246.
(3) Grojtheim, K.; Krohn, C.; Malinovsky, M.; Matiasovsky, K.; Thonstad, J. *Aluminum Electrolysis*, 2nd ed.; Aluminum-Verlag: Dusseldorg, 1982.
(4) Lane, J. A.; MacPherson, H. G.; Maslan, F. *Fluid Fuel Reactors*; Addison-Wesley Publishing Co., Inc.: Reading, MA, 1958.
(5) Broc, M. Etude de revetements metalliques prepares par electrolyse ignee (A Study of Metallic Platings Prepared by Fused Salt Electrolysis). Ph.D. Thesis, Université Pierre et Marie Curie, Paris, 1977. See also Central European Agency Report, No. 4921, 1978.
(6) Senderoff, S.; Mellors, G. W. *J. Electrochem. Soc.* **1965**, *112*, 841−843.
(7) Baraboshkin, A. N.; Saltykova, N. A.; Semenov, B. G. *Tr. Inst. Elektrochim., Ural'. Nauchn. Tsentr, Akad. Nauk SSSR* **1976**, *24*, 28−31.
(8) Butskii, V. D.; Pervov, V. S.; Sevast'yanov, V. G. *Russ. J. Inorg. Chem.* **1977**, *22*, 771−773.
(9) Burgess, J.; Peacock, R. D. *J. Fluorine Chem.* **1977**, *10*, 479−486.
(10) Beuter, A.; Kuhlman, W.; Sawodny, W. *J. Fluorine Chem.* **1975**, *6*, 367−368.
(11) Hargreaves, G. B.; Peacock, R. D. *J. Chem. Soc.* **1957**, 4212−4214.
(12) Hargreaves, G. B.; Peacock, R. D. *J. Chem. Soc.* **1958**, 2170−2175.
(13) Moock, K. H.; Rock, M. H. *J. Chem. Soc., Dalton Trans.* **1993**, 2459−2463.
(14) Sunder, W. A.; Wayda, A. L.; Distefano, D.; Falconer, W. E.; Griffiths, J. E. *J. Fluorine Chem.* **1979**, *14*, 299−325.
(15) Adam, S.; Ellern, A.; Seppelt, K. *Chem.—Eur. J.* **1996**, *2*, 398−402.

10.1021/ic000491o CCC: $20.00
Published on Web 01/12/2001

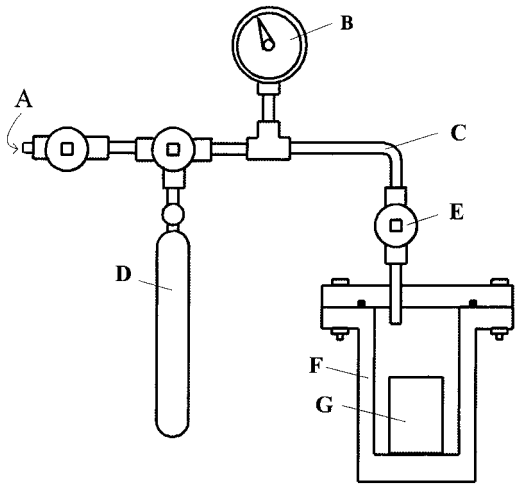

Figure 1. Reaction apparatus for tungsten compounds: (A) Monel gauge for vacuum/pressure; (B) $He-N_2$ vacuum/pressure inlet; (C) Monel tubing; (D) WF_6 gas cylinder; (E) Monel valves; (F) Inconel cell; (G) glassy carbon crucible.

HF and reduce metal ion impurities. This produced FLINAK containing <12 ppm oxide, as determined by the apparatus described previously.[16] Prior to electrochemical measurements, the FLINAK melt was further purified by electrolysis at a Ni plate cathode with an applied potential of −1.5 to −1.8 V. The glassy carbon crucible containing the solution acted as the counter electrode. This procedure generally produced smooth voltammograms with background currents at least 2 orders of magnitude less than the currents due to the tungsten fluorides. When the background currents were large enough to cause interference and could not be removed, the FLINAK was discarded. The observed redox potentials (vs a BN reference electrode containing the Ni^{2+}/Ni couple) indicated that iron (Fe^{3+}/Fe^{2+}, $E^0 = -0.2$ V; Fe^{2+}/Fe, $E^0 = -0.39$ V), chromium (Cr^{2+}/Cr, $E^0 = -0.681$ V), and sometimes nickel ions ($E^0 = 0.0$ V) might be the major sources of contamination.

Reaction/Electrochemical Cell. The nickel/stainless steel reaction cell (ca. 90 mL volume) was made from Inconel pipe to which was welded an Inconel plate to form the cell bottom (Figure 1). Stainless steel (SS) knife-edge flanges (Huntington) were used to cap the cell, and copper or nickel-plated copper gaskets were used to seal the cell at the knife edges. Hoke Inconel diaphragm valves in either straight or tee patterns were used throughout the system except for the WF_6 cylinder valve that was supplied by the vendor. The vacuum/pressure gauge (Ashcroft, 30 in. Hg to 30 psi) was also Monel, which resisted corrosion by the WF_6 gas and byproducts such as HF. An Inconel sheathed chromel−alumel thermocouple was placed on the external face of the bottom of the cell to measure the temperature. The interior cell temperature was assumed to be only 2−3 °C lower than the exterior cell reading, since this temperature difference was found with similar cells in which a thermocouple was inserted directly into the melt.

The crucibles used to contain the reactants at the higher temperatures were in all cases made from glassy carbon (Sigridur G, obtained from EMC Industries, Flemington, NJ) and were from 30 to 50 mL in volume. Helium gas was used to pressurize the system except when the reaction was performed without release of the pressure, in which case the cell contained nitrogen from the inert atmosphere glovebox. All connections were made by either silver-soldering or using Monel Swagelock unions and connectors with Monel ferrules, except where Teflon tubing was used as mentioned in the synthesis procedures.

The cell used for the electrochemical measurements was of similar design except that the volume was ca. 300 mL and that larger glassy carbon crucibles were used. Stainless steel tubes were welded into the top flange to allow the insertion and removal of electrodes, the measurement of temperature, and the addition of chemical samples. These tubes were capped with Swagelock reducing unions (1 to 1/4 in. and 5/8 to 1/4 in.) and cone-shaped Teflon bushings to provide vacuum-tight connections as well as electrical insulation of the electrodes from the cell. The length of the tubes was sufficient to minimize the heat conduction from the cell during operation, which prevented melting of the Teflon bushings. Two Monel diaphragm valves (Hoke) were silver-soldered to 1/4 in. Monel tubing, which was in turn welded to the cell top flange in order to allow gas inlet/outlet flow and regulate the pressure/evacuation of the cell. All connections to the vacuum/pressure system were made with Monel or SS Swagelock fittings and Monel tubing (1/4 in.). The top of the cell usually remained cool enough that additional cooling was not necessary to prevent overheating and seizing of the bolts. The system was pressurized with helium gas at all times except when a vacuum was applied to remove residual hydrogen fluoride gas dissolved in the melt.

Working electrodes for the electrochemical measurements were fabricated by attaching either platinum wire (Aesar, 0.5 mm diam, 99.95%), platinum foil (Aesar, 0.05 and 0.1 mm, 99.95%), tungsten wire (Aesar, 1.0 mm diam, 99.98%), or polished Ni plate to the end of a 1/8 in. nickel rod, which provided exterior electrical connection when inserted through the Teflon bushing. The connections were made by crimping the electrodes into a V-shaped cut in the Ni rod. Immersion depth in the molten FLINAK was determined by measuring the resistance between the glassy carbon crucible and the electrode as the latter was slowly lowered into the cell to determine the point of contact with the melt; upon contact with the melt the resistance dropped to ca. 1.2 Ω. After the electrodes were removed from the melt, the distance was confirmed by measurement of the discoloration on the electrode. The electrodes were generally 2 cm in length or more to avoid contact of the melt with the nickel support rod. Either a glassy carbon rod (Sigridur, grade K, 1 mm diam) or the crucible was the counter electrode. When the glassy carbon crucible was used as the counter electrode, electrical connection was made through the main body of the cell.

Reference electrodes either were platinum foil connected to a nickel rod or were constructed from boron nitride (BN, Advanced Ceramics Corporation and Union Carbide, 1/2 in. diam) as described by Jenkins.[17] However, it was found that BN often gave unreliable potential measurements when tungsten fluorides were added to the melt. This was most likely due to the binder used to hold the BN material together, which was an oxide-containing ceramic. Since the tungsten fluorides were sensitive to the presence of oxide impurities, the BN reference electrodes were subsequently only used to establish the viability of the electrochemical cell apparatus by observing known potentials, such as the Ni^{2+}/Ni couple, and to make reasonable estimates of the metal impurities in the melt before and after electrolysis at a nickel electrode.

X-ray Crystallography. The X-ray crystal structures were determined using a Siemens R3m/V diffractometer fitted with a Nicolet LT-2 low-temperature device. The intensity data were measured with graphite-monochromated Mo Kα radiation ($\lambda = 0.710\,73$ Å). The SHELXTL 93 (versions 5.0 and 5.10) software packages were used to solve (direct methods) and refine the crystal structures. Low-temperature X-ray data were collected on a crystal of K_3WF_6 mounted in paratone oil (Exxon). Crystals of K_2WF_7 were observed to shatter at approximately −25 °C, and thus, room-temperature data were obtained on a crystal encased in epoxy. Although both tungsten salts have large X-ray absorption cross sections, it was not possible to perform analytical corrections to diffraction data based on indexed faces. In the case of K_3WF_6, the low-temperature transfer arms attached to the χ circle prevented orientation of the crystal for face indexing. All attempts to correct for absorption based on faces that were indexed and best estimates of the indices for other faces were not successful. In the case of K_2WF_7, it was very difficult to find a suitable crystal for diffraction studies of this extremely sensitive complex. The crystal chosen was very irregularly shaped, and no analytical absorption model based on face indexing could be found before the crystal decomposed. Therefore, in both cases correction for absorption was made using empirical scan data.

Difference Fourier maps for K_2WF_7 reproducibly showed two areas of low electron density perpendicular to the plane defined by W, F(2), and its symmetry equivalent (Figure 4) in the structure. Thermal

(16) Eklund, S. E.; Toth, L. M.; Chambers, J. Q.; Mamantov, G. *Anal. Chem.* **1999**, *71*, 539−543.

(17) Jenkins, H. W., Jr. Electrochemical Measurements in Molten Fluorides. Ph.D. Thesis, The University of Tennessee, Knoxville, TN, 1969.

Table 1. Syntheses of Alkali Metal Tungsten Fluorides

product	reactants (amount)	conditions	yield (%)
K_2WF_8	KF (5.0 g, 86 mmol) WF_6 gas	870 °C (1 h)	≥97
KWF_7	KF (5.0 g, 86 mmol) WF_6 gas	750 °C (2−3 days)	>60
KWF_6	KF (7.293 g, 25.46 mmol) W (4.680 g, 125.5 mmol) WF_6 gas	850 °C (30 min)	≥97
$NaWF_6$	NaF (4.6 g, 110 mmol) W (3.752 g, 20.41 mmol) WF_6 gas	1050 °C (1 h) 850 °C (2 h)	≥98
$RbWF_6$	RbF (5.21 g, 49.9 mmol) W (5.21 g, 28.3 mmol)	800 °C (2 h)	≥96
$CsWF_6$	CsF (6.03 g, 39.7 mmol) W (3.21 g, 17.4 mmol) WF_6 gas	750 °C (2 h)	≥94
K_3WF_8	KF (4.258 g, 73.29 mmol) KWF_6 (12.324 g, 36.58 mmol)	870 °C (15 min) 800 °C (30 min)	*a*
Na_3WF_8	NaF (12.43 g, 296.0 mmol) $NaWF_6$ (23.63 g, 73.65 mmol) W (9.44 g, 51.34 mmol)	1000 °C (30 min)	<50

[a] A yield of K_3WF_8 was not calculated because the isolated material contained K_2WF_7, as indicated by the Raman spectra.

ellipsoids for F(2) were severely elongated in the direction of these positions when they were not incorporated into the model. A disorder model involving a second pair of fluoride ligands (F(5) and F(6)) at the sites of low electron density was developed. Refinement of the fractional occupancy between these two sets of sites (taking into account special position constraints on site occupation) gave rise to a 0.75/0.25 split. In the disorder model, the thermal ellipsoid parameters for F(2), F(5), and F(6), although still large, were more reasonable than when the disorder was not accounted for in the model. More complicated disorder models did not improve the figures of merit for the overall structure. All residuals and goodness-of-fit parameters improved slightly in the disorder model describe above.

Raman Spectroscopy. All Raman spectra were recorded with a Dilor *XY* CCD detector multichannel spectrometer using the 514 nm line of an Ar ion laser as an excitation source and a laser power between 5 and 100 mW. The samples were sealed in 3 mm square Pyrex tubing (Vitro Dynamics) under vacuum. By careful focusing through a Spex microscope fitted to the Dilor instrument using 10×, 80×, and 100× objectives, the broad background signals at 800 and 450 cm^{-1} due to the glass could be minimized.

Other Instrumentation. The electrochemical instrument used to acquire and record the electrochemical data was an EG&G Princeton Applied Research (PAR) model 273 potentiostat/galvanostat controlled by the PAR M270 Electrochemical Research Software. XPS spectra were obtained using a Perkin-Elmer PHI5000 instrument, which was calibrated using gold and copper standards.

Synthesis of Potassium Octafluorotungstate(VI), K_2WF_8, and Potassium Heptafluorotungstate(VI), KWF_7. These compounds were prepared by the reaction of molten KF with WF_6 gas. Reaction conditions are given in Table 1, and further details can be found elsewhere.[18] The initial rate of reaction was fast because the pressure in the system dropped to 0.0 in. of Hg in less than 2 s when the WF_6 cylinder was closed. The Raman spectra (Figure S1 of Supporting Information and Table 2) of the products were in agreement with the data of Beuter et al.[10] A slight pink coloration, which was evident on occasion, was taken to be indicative of an oxide contamination.

Synthesis of Potassium, Sodium, Rubidium, and Cesium Hexafluorotungstate(V), MWF_6 (M = K, Na, Rb, Cs). This series of compounds was prepared by the reaction of WF_6 with metallic tungsten in a limiting amount of molten MF according to the following reaction:

$$6MF + W + 5WF_6 \rightarrow 6MWF_6 \quad (1)$$

(18) Eklund, S. E. Tungsten fluorides: synthesis and characterization, and electrochemical investigations in the FLINAK molten salt eutectic. Ph.D. Thesis, University of Tennessee, Knoxville, TN, 2000.

Table 2. Raman Bands for Compounds of This Study

compound	frequencies (cm^{-1})
K_2WF_8	667 (strong), 419, 389
KWF_7	716 (strong), 665, 615, 535, 435, 327, 220 (weak)
K_2WF_7	642 (strong), 398 (weak), 250 (broad)
Rb_2WF_7	637 (strong)
KWF_6	702 (strong), 225 (broad, weak)
$NaWF_6$	712 (strong)
$RbWF_6$	696 (strong), 212 (weak)
$CsWF_6$	692 (strong), 209 (weak)
K_3WF_8	598 (strong), 435 (weak), 362
Na_3WF_8	614 (strong), 411 (weak), 372 (weak)
Rb_3WF_8	595 (strong), 428 (weak), 335 (weak)
K_3WF_6	565 (strong), 198 (weak)
Na_3WF_6	585 (strong)

Conditions are given in Table 1 and elsewhere.[18] These products, which were yellow, deomposed slowly with trace moisture in the glovebox to a dark-blue material indicative of the well-known "tungsten blues", such as W_2O_5 and W_4O_{11}. The yellow material did not discolor when it was carefully stored in sealed glass vials. In addition to the KWF_6, a small amount of K_2WF_8 (identified by Raman spectrum) condensed on the cell top. The Raman spectra (Figure S2 of Supporting Information, Table 2) of these compounds exhibited strong υ_1 bands in the region of 690−700 cm^{-1} and much weaker υ_5 bands at 210−225 cm^{-1}, in agreement with the literature.[19,20] Weak bands around 990 cm^{-1} in the spectra are attributed to oxide impurities.[21]

Synthesis of Potassium Heptafluorotungstate(V), K_2WF_7. This compound, which was obtained by the addition reaction of KWF_6 and KF, has not been synthesized previously and represents the first MF_7^{2-} complex of the group VI transition metals. In a typical procedure, 2.032 g (34.97 mmol) of KF and 12.45 g (36.95 mmol) of KWF_6 were added to the reaction cell, which was heated under vacuum at 850 °C for 1 h. The temperature was then decreased to 800 °C, while the vacuum was maintained for approximately 14 h. Then the temperature was decreased to 600 °C over 8 h, followed by rapid cooling to room temperature. Orange crystals (density 3.87 g/cm^3) were isolated from the solidified reaction mixture in approximately 40−50% yield. Anal. Calcd for K_2WF_7: K, 19.79; W, 46.54. Found: K, 20.05; W, 47.55.

The Raman spectrum of the orange K_2WF_7 crystals is shown in Figure 2 along with the Raman spectra of Rb_2WF_7 and K_2TaF_7 for comparison. The principal band appears at 642 cm^{-1}; weaker bands at 398 and 250 cm^{-1} can be assigned to W−F bending modes by analogy to the K_2TaF_7 spectrum.[22] Suitable crystals for an X-ray structure determination were mounted at room temperature on a glass fiber after coating them with epoxy glue. The crystal data for K_2WF_7 are collected in Tables 3−5.

When the synthesis of Rb_2WF_7 was carried out at 800 °C in the same manner as above, a light-pink crystalline material was obtained that appeared to be a mixture of compounds. In addition to the pink material, a green material (possibly Rb_3WF_8; see below) along with some orange-brown material was formed in a pocket of the product boule. The Raman spectrum of the pink material featured a prominent band at 637 cm^{-1}, which is in the range expected for Rb_2WF_7(vide infra), along with a significant oxide band at 973 cm^{-1}.

Synthesis of Potassium, Sodium, and Rubidium Octafluorotungstate(V), M_3WF_8 (M = K, Na, Rb). These compounds were obtained by the addition reaction of molten MF and MWF_6 (see Table 1) via the following reaction:

$$MWF_6 + 2MF \rightleftarrows M_3WF_8 \quad (2)$$

The isolated potassium salt of the eight-coordinate tungstate(V) fluoride contained some seven-coordinate WF_7^{2-} ions, as indicated by the Raman spectra, and the Rb_3WF_8 was obtained as a byproduct (yield, ca. 5%) of the Rb_2WF_7 procedure described above.

(19) Anderson, G. M.; Iqbal, J.; Sharp, D. W. A.; Winfield, J. M.; Cameron, J. H.; McLeod, A. G. *J. Fluorine Chem.* **1984**, *24*, 303−317.
(20) Shamir, J.; Malm, J. G. *J. Inorg. Nucl. Chem. Suppl.* **1976**, 107.
(21) Beuter, A.; Sawodny, W. *Z. Anorg. Allg. Chem.* **1976**, *424*, 37−44.
(22) Torardi, C. C.; Brixner, L. H.; Blasse, G. *J. Solid State Chem.* **1987**, *67*, 21−25.

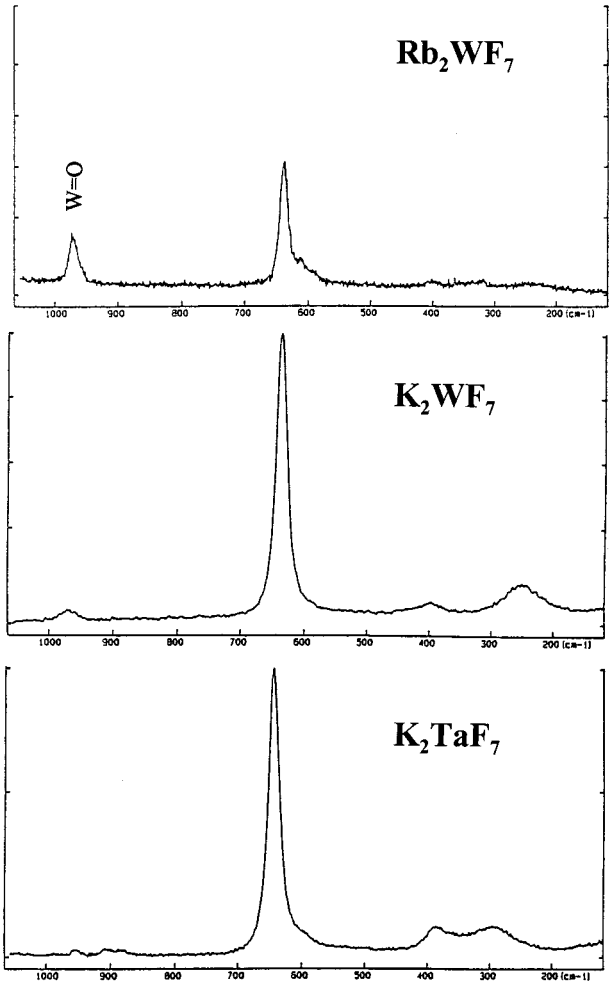

Figure 2. Raman spectra of Rb_2WF_7, K_2WF_7, and K_2TaF_7.

Table 3. Crystal Data and Structure Refinement for K_2WF_7 and K_3WF_6

	K_2WF_7	K_3WF_6
fw	395.05	415.15
a (Å)	9.800(2)	8.9160(10)
b (Å)	5.7360(11)	8.9160(10)
c (Å)	11.723(2)	8.9160(10)
$\alpha = \beta = \gamma$ (deg)	90	90
V (Å^3)	659.0(2)	708.78(14)
Z	4	4
space group	*Pnma* (No. 62)	$Fm\bar{3}$ (No. 225)
λ (Å)	0.710 73	0.710 73
temp (K)	293(2)	173(2)
ρ_{calc} (Mg/m^3)	3.982	3.890
μ (cm^{-1})	18.854	18.093
R [a] (F_o^2; all data)	0.0539	0.0435
R_w^2 [a] (F_o^2; all data)	0.0964[b,d]	0.1304[c,d]

[a] $R = \sum||F_o| - |F_c||/\sum|F_o|$. $R_w^2 = [\sum w(|F_o| - |F_c|)^2/\sum w|F_o|^2]^{1/2}$. [b] $w = 1/[\sigma^2(F_o^2) + (0.0277P)^2 + 17.23P]$. [c] $w = 1/[\sigma^2(F_o^2) + (0.0797P)^2 + 12.15P]$. [d] $P = (F_o^2 + 2F_c^2)/3$.

These compounds, which were green, exhibited a principal strong Raman band in the region 595−614 cm^{-1} and two weaker bands at 411−435 and 335−372 cm^{-1} (Figure S3 of Supporting Information and Table 2). The Raman spectrum of the K_3WF_8 contained a band at 642 cm^{-1}, with an intensity of approximately 20% of the 598 cm^{-1} band, at the same frequency as the υ_1 band for the WF_7^{2-} species (Figure 2). This latter band was not present in the room-temperature spectrum of frozen FLINAK containing the green solid, indicating the presence of WF_8^{2-} alone in the presence of excess MF.

The salt Na_3WF_8 was actually isolated from a reaction mixture containing metallic tunsgten powder and excess NaF in an attempt to prepare lower oxidation state tungsten fluorides (see synthesis of K_3WF_6 below). The Raman spectrum (Figure S3), which indicated the salt to be quite pure, was strikingly similar to that of Na_3TaF_8.[23]

Table 4. Atomic Coordinates ($\times 10^4$) and Equivalent Isotropic Displacement Parameters (Å$^2 \times 10^3$) for K_2WF_7[a]

	x	y	z	U(eq)
W(1)	7544(1)	2500	3709(1)	23(1)
K(1)	8637(5)	7500	5603(4)	30(1)
K(2)	5519(6)	2500	6684(5)	44(1)
F(1)	9003(11)	220(15)	3700(9)	57(3)
F(4)	6476(14)	260(20)	4551(13)	103(5)
F(3)	8270(30)	2500	5253(16)	119(9)
F(2)	6890(30)	420(30)	2593(15)	154(18)
F(5)	8280(80)	2500	2170(50)	130(40)
F(6)	5680(80)	2500	3130(50)	130(40)

[a] U(eq) is defined as one-third of the trace of the orthogonalized U_{ij} tensor.

Table 5. Selected Bond Lengths [Å] and Angles [deg] for K_2WF_7

Bond Distances			
W(1)−F(1)	1.937(10)	K(1)−F(4)#4	2.917(16)
W(1)−F(2)	1.882(16)	K(1)−F(3)	2.920(4)
W(1)−F(3)	1.943(19)	K(1)−F(6)#3	3.03(6)
W(1)−F(4)	1.929(12)	K(2)−F(1)#6	2.870(11)
W(1)−F(5)	1.94(6)	K(2)−F(4)#7	2.902(16)
W(1)−F(6)	1.95(7)	K(2)−F(4)	2.965(16)
W(1)−K(1)	3.782(3)	K(1)−F(5)#3	2.62(7)
W(1)−K(1)#1	3.782(3)	K(2)−F(2)#7	3.02(3)
W(1)−K(1)#2	3.820(5)	K(2)−F(6)#11	3.11(3)
K(1)−F(5)#3	2.62(7)	K(2)−F(5)#3	3.15(3)
K(1)−F(2)#3	2.670(16)	F(3)−K(1)#5	3.20(3)
K(1)−F(1)#4	2.747(10)	F(2)−K(2)#11	3.02(3)
K(1)−F(1)#5	2.780(12)	F(2)−K(2)#13	3.22(3)

Angles			
F(2)−W(1)−F(2)#4	78.6(10)	F(1)#4−W(1)−F(1)	84.9(6)
F(2)−W(1)−F(4)	75.5(9)	F(2)−W(1)−F(3)	140.5(5)
F(2)−W(1)−F(4)#4	126.4(11)	F(4)#4-W(1)−F(3)	73.8(8)
F(2)#4−W(1)−F(4)#4	75.5(9)	F(1)#4−W(1)−F(3)	74.7(7)
F(4)−W(1)−F(4)#4	83.6(8)	F(2)#4−W(1)−F(5)	58.6(16)
F(2)−W(1)−F(1)#4	132.4(9)	F(4)−W(1)−F(5)	132.5(10)
F(2)#4−W(1)−F(1)#4	79.6(9)	F(3)−W(1)−F(5)	137(2)
F(4)−W(1)−F(1)#4	148.5(6)	F(2)−W(1)−F(6)	55.9(14)
F(4)#4−W(1)−F(1)#4	87.3(5)		

The material that gave the Raman spectrum in Figure S3, assigned to the Rb_3WF_8 compound, was isolated as a byproduct of the preparation of Rb_2WF_7 in less than 5% yield. The isolated material contained a significant fraction of seven-coordinate WF_7^{2-} and a significant oxide impurity indicated by the presence of a band at 956 cm^{-1}.

Synthesis of Potassium Hexafluorotungstate(III) Fluoride, K_3WF_6. The synthesis of this compound was attempted by reduction of K_3WF_8 with tungsten metal via the following reaction:

$$3K_3WF_8 + 2W + 6KF \rightarrow 5K_3WF_6 \qquad (3)$$

Although the bulk of the isolated material was a mixture of K_3WF_8 and K_3WF_6, a small amount of a crystalline product, suitable for X-ray structure determination, was isolated and identified as K_3WF_6. Two procedures were followed: in one the reaction mixture was under vacuum, and in the other the pressure was allowed to build up. In the former, 5.03 g (11.1 mmol) of K_3WF_8, 1.32 g (22.7 mmol) of KF, and 4.57 g (24.9 mmol) of W was heated to 810 °C for approximately 16 h. The bulk of the product isolated from the cell at room temperature was a dark-brown solid that was shown by its Raman spectrum to be close to a 50−50 mixture of K_3WF_8 and some other compound. Above the main boule of brown material, at the ends of KF dendrites that had condensed from the vapor state, translucent green crystals had formed (yield, <1%). This compound was shown to be K_3WF_6 by its X-ray crystal structure. The crystal data and summaries of atomic coordinates, bond lengths, and bond angles are given in Tables 3, 6, and 7.

In the second procedure, a mixture of 14.80 g (32.7 mmol) of K_3WF_8, 5.268 g (90.67 mmol) of KF, and 5.20 g (28.3 mmol) of tungsten powder was heated to 800 °C for 3 days without relieving the pressure buildup. When the reaction vessel was opened after slow cooling to room temperature, three distinct layers were present. The bottom two

Table 6. Atomic Coordinates ($\times 10^4$) and Equivalent Isotropic Displacement Parameters ($Å^2 \times 10^3$) for K_3WF_6[a]

	x	*y*	*z*	*U*(eq)
K(2)	5000	10000	0	71(6)
W	5000	5000	0	48(2)
K(1)	7500	7500	2500	83(5)
F(1)	2970(40)	5000	0	250(30)

[a] *U*(eq) is defined as one-third of the trace of the orthogonalized U_{ij} tensor.

Table 7. Selected Bond Lengths [Å] and Angles [deg] for K_3WF_6

Bond Distances			
K(2)−F(1)#1	2.65(3)	W−K(1)	3.8607(4)
K(2)−K(1)	3.8607(4)	K(1)−F(1)#2	3.180(4)
W−F(1)	1.81(3)	F(1)−K(2)#3	2.65(3)
Bond Angles			
F(1)#4−K(2)−F(1)#1	90.0	F(1)#10−W−F(1)	180.0
K(1)#5−K(2)−K(1)#6	180.0	F(1)#11−W−F(1)	90.0
F(1)#1−K(2)−K(1)#7	54.7	F(1)#10−W−K(1)	54.7
F(1)#8−K(2)−K(1)	54.736(2)	F(1)−W−K(1)	125.3
K(1)#6−K(2)−K(1)	109.5	F(1)−W−K(1)#10	54.7
K(1)#9−K(2)−K(1)	70.5	F(1)#11−W−K(1)#12	125.264(1)

layers were brown, the bottom darker than the middle layer, and the top layer was a cloudy white with a greenish tint (possibly phase-separated KF and green K_3WF_8). Unreacted shiny, flat tungsten metal layers (identified by XPS spectra) were embedded throughout the brown material, which indicated the disproportionation of an intermediate to tungsten metal and a higher oxidation state.

In a similar procedure, 7.17 g of a dark-brown product was obtained when 5.30 g (13.1 mmol) of Na_3WF_8 and 3.10 g (16.9 mmol) of NaF were heated at 850 °C for 5 h. The major loss of material was due to a condensate of $NaWF_6$ (identified by its Raman spectrum) that had formed on the cell top consistent with the following reaction:

$$6Na_3WF_8 + 2W \rightarrow 5Na_3WF_6 + 3NaWF_6 \qquad (4)$$

The Raman spectra of the brown products of these reactions (Figure 3) revealed the fingerprint bands for K_3WF_8 and Na_3WF_8 at 599 and 361 cm^{-1} and 615 and 375 cm^{-1}, respectively. A second set of bands associated with an unknown component can be seen at 565 and 198 cm^{-1} for the potassium salt mixture and one band at 585 cm^{-1} for the sodium salt mixture. In addition bands in the 960−980 cm^{-1} region, which were always present in the spectra of the brown material, indicated a minor oxide impurity. As discussed below, the unknown component of these mixtures is likely to be M_3WF_6. An X-ray powder diffraction pattern of the brown material showed a slight splitting of the peaks, indicating the presence of two distinct unit cells, the larger agreeing with the cell size of K_3WF_8.

Results and Discussion

Crystal Structures. ORTEP drawings of the structures of the two new potassium tungsten fluorides prepared in this study are shown in Figures 4 and 5. In the K_2WF_7 structure, the tungsten atom is surrounded by an array of seven fluoride ligands in a distorted trigonal prism where one of the rectangular faces is capped by the seventh fluoride ion. Two of the fluoride ligands are unequally disordered between two sets of positions {F(2)/F(2′) and F(5)/F(6)} around the tungsten and exhibit large thermal parameters (see Experimental Section). The seven W−F bond lengths are in the range 1.88(2)−1.94(2) Å. Each WF_7 unit is accompanied by two crystallographically nonequivalent 11-coordinate K^+ ions, with K−F distances ranging from 2.67(2) to 3.22(3) Å. This is in contrast to the K_2TaF_7[22] and K_2NbF_7[24] structures, both of which contain 9-coordinate potassium ions.

The structure of K_3WF_6 is isomorphous with that of the molybdenum analogue K_3MoF_6 previously reported by Toth et al.;[25] the initial model for refinement of the K_3WF_6 structure

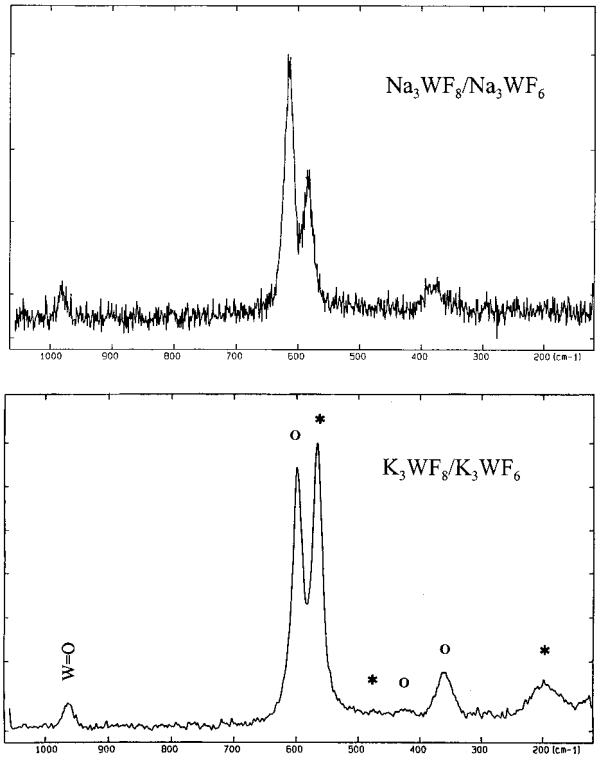

Figure 3. Raman spectra of Na_3WF_8/Na_3WF_6 and K_3WF_8/K_3WF_6 mixtures: (○) K_3WF_8; (∗) K_3WF_6.

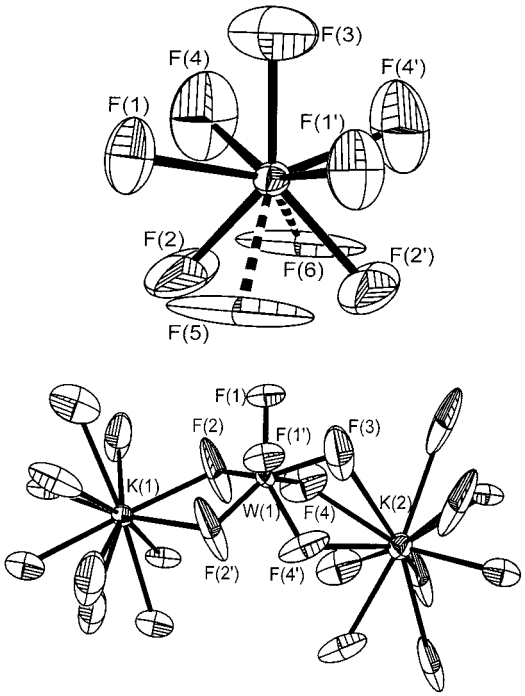

Figure 4. ORTEP diagrams for K_2WF_7 and K_3WF_6. Thermal ellipsoids represent 50% probabilities. In the structure of K_2WF_7, F(2)/F(2′) (major) and F(5)/F(6) (minor) constitute a set of two disordered fluoride ligands around the tungsten. See Experimental Section for details concerning the structural models and refinement results.

was based on the coordinates of the molybdenum species. The fluorine anisotropic temperature factors normal to the W−F bond are abnormally large (Table S5 of Supporting Information). Similar behavior has been observed in the structures of isomorphous analogues to K_3WF_6. The possibility that such large

(23) Hartman, K. O.; Miller, F. A. *Spectrochim. Acta A* **1968**, *24*, 669.

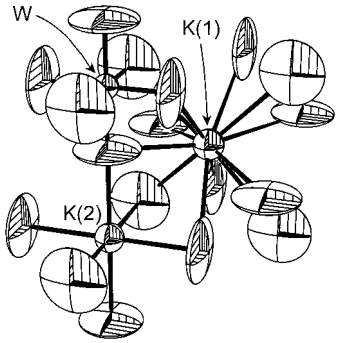

Figure 5. ORTEP diagram for K_3WF_6. Thermal ellipsoids represent 50% probability.

thermal parameters represent a random spatial disorder of the fluorine around the special position it resides on has been discussed.[25] As observed previously, attempts to model such disorder were unsuccessful in the case at hand, and the simplest model for the system was chosen.

The tungsten atom coordination is a perfect octahedron with 1.81(3) Å W−F bond distances. The unit cell contains alternating WF_6 and KF_6 octahedrons in a NaCl-like arrangement. The K−F bond distances are 2.65(3) Å, and there are an additional eight K^+ ions per unit cell, which are coordinated to 12 F^- ions in a distorted cubic octahedral array with K−F distances of 3.8607(4) Å.

Raman Spectra. The Raman spectra of the tungsten fluorides prepared in this study (Figures 2, 3, and S1−S3) feature a prominent, intense band in the region 565−715 cm^{-1} that can be assigned to a symmetric stretching mode of the complex ion. For the six-coordinate MWF_6 compounds this band can be readily assigned to the $\upsilon_1(A_{1g})$ breathing mode of an octahedral complex. In addition, a much weaker $\upsilon_5(F_{2g})$ scissoring mode was present in the spectra in the 200 cm^{-1} region. Polarized Raman spectra (not shown) indicated that this band was buried under the broad band seen in the 200−225 cm^{-1} in the KWF_6 spectrum of Figure S2. The $\upsilon_2(E_g)$ vibration, which has been reported at 470 cm^{-1} for the gas-phase spectrum of WF_6^-,[9] was not seen presumably because of suppression by solid-state effects.

Identification of the unknown components of the solid-state mixtures that gave the spectra of Figure 3 as M_3WF_6 is supported by the correlations seen in Figures 6 and 7. In Figure 6, the correlation among coordination number, oxidation state, and the frequency of the principal stretching mode of the complex is seen. Figure 7 shows that the υ_1, υ_2, and υ_5 bands for the presumed K_3WF_6 compound are in complete accord with the frequencies of the bands for known WF_6 and KWF_6 compounds. This strongly supports our assignment of M_3WF_6 (M = Na, K) to the unknown component of the brown product mixtures.

Electrochemistry. Cyclic voltammograms were obtained for all of the above compounds in molten FLINAK at platinum working electrodes. In addition Raman spectra were obtained on the frozen FLINAK mixtures in order to ascertain the principal species in the melt by comparison with the spectra of the known compounds in Figures 2, 3, S1, and S2. Only the potassium and sodium tungsten fluoride salts were used in these studies so that no new cations were introduced into the melt. Emphasis was placed on the voltammetry of the W(V) complexes, which produced the most clearly defined electrochemical responses. Since all of the voltammetry in FLINAK was plagued by the presence of oxides, the effect of added Na_2O was also determined.

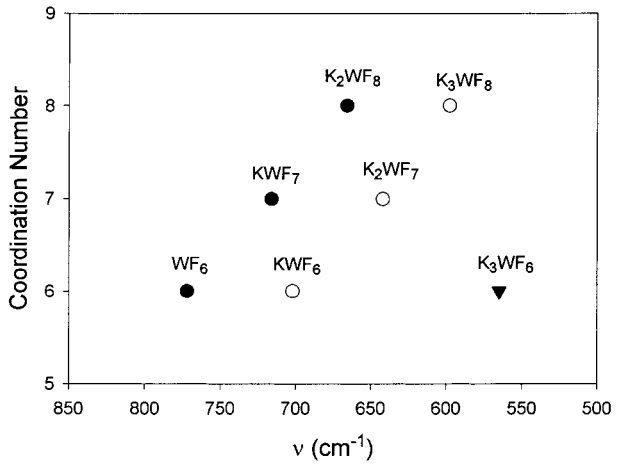

Figure 6. Main band frequency shift with change in oxidation state and fluoride coordination number.

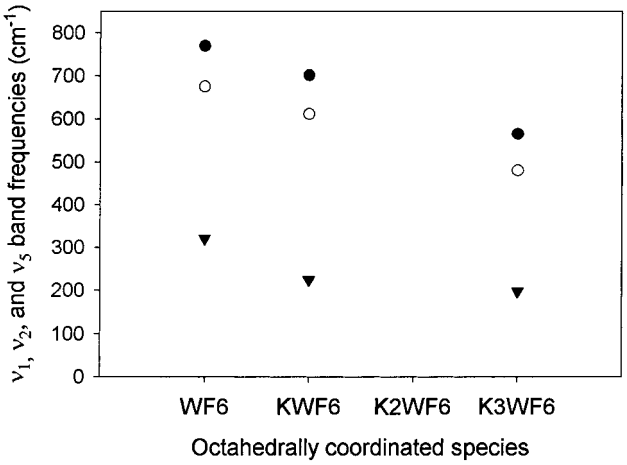

Figure 7. Relationship of main band Raman frequencies for octahedrally coordinated tungsten fluorides: (●) υ_1 band; (○) υ_2 band; (▼) υ_5 band.

Raman spectra of all of the W(V) species in FLINAK were nearly identical, showing the main band at 598 cm^{-1} for the WF_8^{3-} species. The band for WF_7^{2-} at 637 cm^{-1} was barely discernible, there was no evidence for the WF_6^- species, and all three W(V) compounds (K_3WF_8, K_2WF_7, and KWF_6) gave similar cyclic voltammetry. These observations indicate that WF_8^{3-} is the principal W(V) species present in the FLINAK melt.

The voltammogram of Figure 8 exhibits at least two reduction waves (R_1 and R_2) and a sharp W metal anodic stripping wave in the region 0.3−0.4 V vs the quasi-Pt reference. The voltammetry of the tungsten fluorides in FLINAK is remarkably similar to previously reported voltammograms for other refractory metals in this medium.[26−29] Assignment of the anodic process in Figure 8 to oxidation of electrodeposited tungsten is consistent with these previous studies and with the voltammetric corrosion of a tungsten wire electrode depicted in Figure S4 of Supporting Information. Besides showing that the anodic dissolution of W occurs in the 0.4 V region, the voltammogram of Figure S4 also provides a rough calibration of the Pt quasi-reference electrode because the Li^+/Li metal couple is seen at −1.8 V.

(24) Brown, G. M.; Walker, L. A. *Acta Crystallogr.* **1966**, *20*, 220−229.
(25) Toth, L. M.; Brunton, G. D.; Smith, G. P. *Inorg. Chem.* **1969**, *8*, 2694−2697.

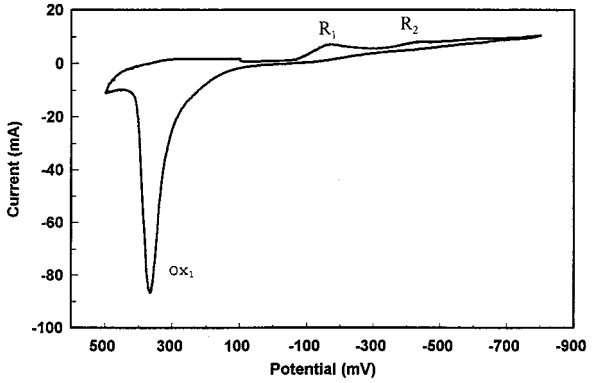

Figure 8. Cyclic voltammogram of K_3WF_8 in FLINAK, 540 °C: A_{Pt} = 0.157 cm^2, scan rate = 100 mV/s, Pt quasi-reference electrode, glassy carbon crucible counter electrode.

When the negative potential sweep was restricted to the R_1 wave, integration of the cathodic current in all instances gave a cathodic charge equal to the anodic charge under the tungsten metal stripping wave. This indicates that the R_1 current is due to a five-electron reduction to tungsten metal:

$$WF_8^{3-} + 5e^- \rightarrow W + 8F^- \qquad (5)$$

A similar conclusion was reached by Polyakova et al. for the reduction of K_2TaF_7 in FLINAK.[27]

Assignment of wave R2 in the voltammogram of Figure 8 to reduction of an oxide species is supported by the voltammograms obtained when Na_2O was purposefully added to the melt. As the oxide content was increased, wave R2 increased at the expense of R1. This behavior also has precedence in the Ta(V) FLINAK system.[27] An example is shown in Figure S5 of Supporting Information where the oxide/W ratio is 0.76. At higher oxide concentration, R1 is difficult to distinguish from the presumed tungsten oxide reduction current and the anodic stripping wave is diminished and broadened considerably.

When the temperature of the WF_8^{3-}/FLINAK melts was increased, a prewave (R0) became evident at potentials positive of the R1 wave (Figure 9). Concurrent with the growth of the prewave, the anodic stripping wave became much more structured with up to three peaks evident at potentials positive of the main anodic peak. Formation of a W(Pt) alloy layer in the electrodeposition process is a possible explanation for this behavior. In this case, the overpotential barrier(s) that gives rise to the stripping wave structure is due to the energy required to break the Pt−W bonds. The inset in Figure 9 shows a plot of $\ln(I_{pk}T^{1/2})$ where I_{pk} is the maximum current and T is the absolute temperature. If the temperature dependence of the current is primarily due to diffusion of the tungsten fluoride complex, the slope of this plot gives an estimate of the activation energy for diffusion. For an irreversible reaction that obeys the Randles−Sevcik equation,

$$I_{pk}T^{1/2} = 0.496nFAC^b\upsilon^{1/2}(\alpha n_aF/R)^{1/2}D^{1/2} \qquad (6)$$

the slope of the log plot is $E_{act}/(2RT)$, which results in an activation energy of diffusion equal to 58.9 ± 1.4 kJ/mol for the data of Figure 9.

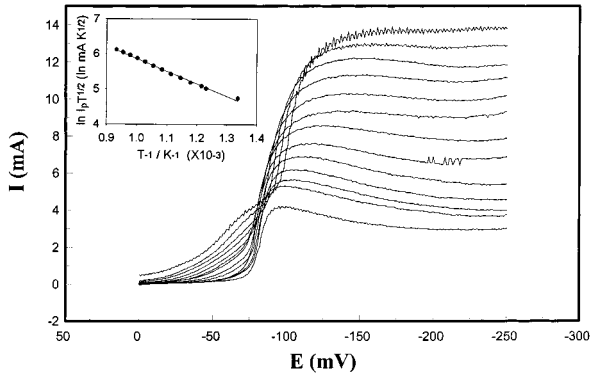

Figure 9. Voltammograms showing increasing current with increasing temperature: T = 475, 535, 550, 575, 600, 625, 650, 675, 700, 725, 750, 775, and 800 °C; A_{pt} = 0.157 cm^2; scan rate = 100 mV/s; $C_{W(V)}$ (at 500 °C) = 5.20 × 10^{-5} M (0.0990 mol %). Inset: variation of $\ln I_pT^{1/2}$ with T^{-1}; E_{act} = 58.9 ± 1.4 kJ/mol.

For the K_3WF_8/FLINAK system, temperatures between 600 and 700 °C produced cyclic voltammograms with the "cleanest" anodic stripping pattern and minimal distortion of the R1 wave by the R0 prewave. On this basis, this temperature range is suggested for electrodeposition of tungsten on platinum.

Addition of the brown solid believed to be a mixture of K_3WF_8 and K_3WF_6 to FLINAK produced cyclic voltammograms very much identical to those obtained with the pure green K_3WF_8 compound. This is consistent with the Raman spectra obtained on FLINAK melts containing increasing amounts of the brown solid (Figure 10). At low concentration the peaks assigned to K_3WF_8 and K_3WF_6 were present in roughly equal amounts, and as the concentration was increased, the K_3WF_8 peak is seen to dominate the K_3WF_6 peak. This indicates that comproportionation of WF_8^{3-} and metallic W occurred in the fluoride-rich melt to form WF_6^{3-}:

$$3WF_8^{3-} + 2W + 6F^- \rightleftarrows 5WF_6^{3-} \qquad (7)$$

and that a $[WF_6^{3-}]/[WF_8^{3-}]$ equilibrium ratio close to unity existed under these conditions. Accordingly, the potentials of the W(V/III) and W(III/0) couples will be close to each other in the melt. Note that excess W metal is likely to be present as an impurity in the brown solid and that for the spectra of Figure 10 excess W metal was added on purpose. Also, the concentration dependence seen in Figure 10 is in accord with the law of mass action for the above equilibrium if the fluoride activity is constant in the FLINAK melt. This equilibrium would also account for the noninteger oxidation states seen by previous workers in the tungsten/FLINAK system.

The voltammetry of the brown K_3WF_8/K_3WF_6 material in FLINAK again revealed the problem of oxide impurity. In the absence of added Na_2O, a poorly formed reduction wave was observed with R1 and R2 components similar to those of Figures 8 and S5. Identical behavior was seen when the sodium salt mixture was used. Upon addition of oxide to the melt, wave R1 was suppressed and the anodic stripping wave broadened and became less intense. At a 2:1 molar ratio of oxide/W, no Faradaic current was seen in the region of 0.0 to −1.0 V, indicating that the tungsten oxides are electroinactive at these potentials in FLINAK.

Summary

As shown in this study, molten fluorides are a viable medium for syntheses of refractory metal complexes and their alkali

(26) Van, V.; Silny, A.; Hives, J.; Danek, V. *Electrochem. Commun.* **1999**, *1*, 295−300.
(27) Polyakova, L. P.; Polyakov, E. G.; Matthiensen, F.; Christensen, E.; Bjerrum, N. J. *J. Electrochem. Soc.* **1994**, *141*, 2982−2988.
(28) Clayton, F. R.; Mamantov, G.; Manning, D. L. *J. Electrochem. Soc.* **1974**, *121*, 86−90.
(29) Taxil, P.; Mahenc, J. *J. Appl. Electrochem.* **1987**, *17*, 261−269.

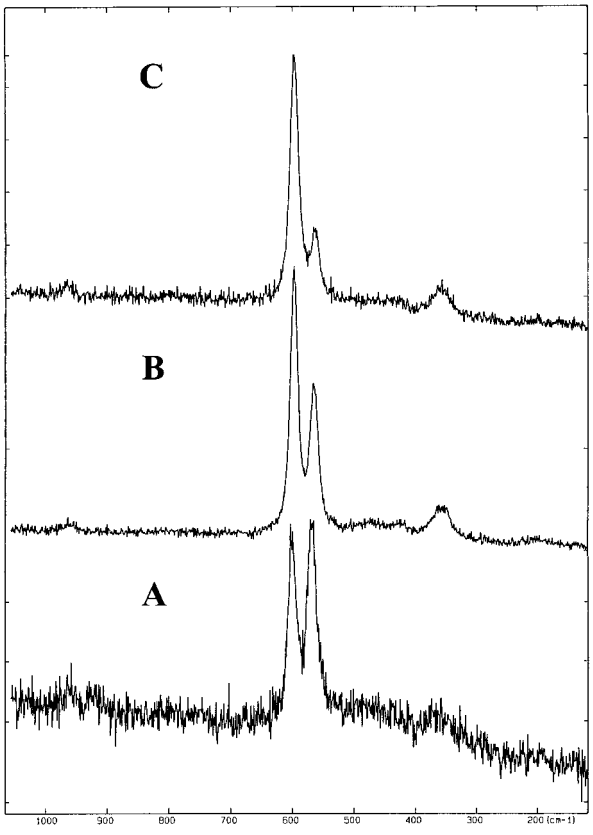

Figure 10. Variation in K_3WF_8 (598 cm^{-1}) and K_3WF_6 (565 cm^{-1}) Raman band intensities in a solidified FLINAK melt with increasing addition of WF_6 in a bath containing excess W metal: (A) 1.12, (B) 4.21, and (C) 6.29 mol % WF_6.

metal salts. While high-temperature conditions and inert atmosphere manipulations are required, these difficulties are offset by the facile kinetics, high yields, and simple isolation procedures that are realized. Care must be taken, however, to minimize the level of oxide impurities, which affects both the synthetic methods and the electrochemical behavior.

While the voltammetry of the tungsten electrodeposition process in FLINAK suggested that reduction of W(V) proceeded via an overall five-electron process, it is likely that a W(III) species such as WF_6^{3-} is formed as a two-electron intermediate in this process. Since the latter species was indicated as an equilibrium component of the K_3WF_8/W mixture in FLINAK by the Raman spectra, it is also likely to be present in the diffusion layer at a freshly deposited tungsten metal layer in this same medium. Further studies, e.g., rotating ring-disk voltammetry, are indicated in order to more fully understand the role of WF_6^{3-} in the electrodeposition process.

Acknowledgment. This work was supported by a contract with Lockheed Martin Energy Systems, Inc. and AFOSR for a fellowship to Sven Eklund. Dr. L. M. Toth (ORNL) provided much useful guidance on the high-temperature molten salt chemistry. We also gratefully acknowledge several critical insights provided by a reviewer and Dr. Jeff C. Bryan (ORNL) in developing the model for the structure of K_2WF_7. Charmaine Mamantov and Haiming Xiao are also thanked for many helpful discussions.

Supporting Information Available: Listings of bond lengths and angles, anisotropic displacement parameters, structure factors, and X-ray crystallographic files in CIF format for the structure determinations of K_2WF_7 and K_3WF_6; Raman spectra of K_2WF_8, KWF_7, MWF_6 (M = Na, K, Rb and Cs), and M_3WF_8 (M = Na, K and Rb); cyclic voltammograms of (1) a tungsten wire and (2) K_3WF_8 upon addition of oxide in FLINAK. This material is available free of charge via the Internet at http://pubs.acs.org.

IC000491O